Improved Pd electro-catalysis for oxygen reduction reaction in direct methanol fuel cell by reduced graphene oxide

R. Carrera-Cerritos [a,g], V. Baglio [b,*], A.S. Aricò [b], J. Ledesma-García [c], M.F. Sgroi [d], D. Pullini [d], A.J. Pruna [e,f,**], D.B. Mataix [f], R. Fuentes-Ramírez [a], L.G. Arriaga [g,***]

[a] Departamento de Ingeniería Química, Universidad de Guanajuato, División de Ciencias Naturales y Exactas, Noria Alta s/n, Col. Noria Alta, Guanajuato, Gto., C.P. 36050, Mexico
[b] Istituto di Tecnologie Avanzate per l'Energia "Nicola Giordano", CNR, Via Salita S. Lucia Sopra Contesse 5, Messina, Italy
[c] Facultad de Ingeniería, División de Investigación y Posgrado, Universidad Autónoma de Querétaro, Centro Universitario Cerro de las Campanas, Querétaro, Qro., C.P. 76010, Mexico
[d] Centro Ricerche Fiat, Orbassano (TO), Italy
[e] University of Bucharest, 405 Str. Atomistilor, Magurele, Ilfov, Romania
[f] Universidad Politécnica de Valencia, Camino de Vera s/n, 46022 Valencia, Spain
[g] Centro de Investigación y Desarrollo Tecnológico en Electroquímica, Parque Tecnológico Querétaro s/n, Sanfandila, Pedro Escobedo, Qro., C.P. 76703, Mexico

ARTICLE INFO

ABSTRACT

Noble metallic nano-catalysts supported on carbon based substrates are extensively used as electrodes for direct methanol fuel cells (DMFCs). Pd is a promising alternative to the more expensive Pt whether its catalytic properties should be improved. To this aim, reduced graphene oxide (rGO) was employed in this study as an alternative to conventional carbon black (C) substrates to improve the catalytic properties of Pd. Pd nanobars and Pt nanoparticles were synthesized, by the polyol method, and deposited for comparison both on commercial carbon and rGO. The oxygen reduction reactions (ORRs) at the fabricated electrodes were tested by the Rotating Disk Electrode (RDE) technique in acidic media. To correlate the activity to other physico-chemical properties, the nano-catalysts were characterized by Thermo Gravimetric Analysis (TGA), X-Ray Diffraction (XRD), and Transmission Electron Microscopy (TEM). The electro-catalytic activity of the electrode is importantly affected by the support chosen. Specifically, the Pd nano-catalyst proved an enhanced performance when on rGO, while the Pt counterpart was found being more active when placed on C. This result can be explained with a strong dependence of the ORR on the interaction between the metal nano-catalyst and the carbon based support.

© 2013 Elsevier B.V. All rights reserved.

1. Introduction

Thanks to negligible emissions of CO_2 and high energy densities, Proton Exchange Membrane (PEM) fuel cells fed with hydrogen or organic molecules are acknowledged as being a promising power source suitable to replace internal combustion engines in nowadays vehicles [1]. On the contrary, the high cost and scarce reliability of such a system limit their commercialization. The availability of novel low cost electro-catalysts suitable to replace the expensive platinum can pave the way for the penetration of PEM in the market [2]. In this regard, extensive research of non-Pt catalysts for oxygen reduction reaction (ORR) has been conducted, and today, a wide range of alternative materials to replace platinum are reported [3–5]. Despites of claims, the activities for the ORR of literature materials are significantly lower than platinum's. Palladium is a promising candidate among them, although its catalytic ability at fully reducing oxygen into water with low over-potential and low hydrogen peroxide (or peroxy-radicals) production has still to be improved. Palladium has valence shell electronic configuration and lattice constant similar to Pt [3]. For both aspects, Pd can be a viable alternative material for low-temperature fuel cells. In addition, the price for troy ounce of Pd is practically five times lower than the price of platinum. Moreover, the abundance of Pd on Earth

* Corresponding author at: Istituto di Tecnologie Avanzate per l'Energia "Nicola Giordano", CNR, Via Salita S. Lucia Sopra Contesse 5, 98126 Messina, Italy. Tel.: +39 090 624237; fax: +39 090 624247.
** Corresponding author at: University of Bucharest, 405 Str. Atomistilor, Magurele, Ilfov, Romania. Tel.: +34 627018518.
*** Corresponding author. Tel.: +52 442 211 6069; fax: +52 442 211 6001.
E-mail addresses: vincenzo.baglio@itae.cnr.it (V. Baglio), ai.pruna@gmail.com (A.J. Pruna), larriaga@cideteq.mx (L.G. Arriaga).

is two hundred times higher than Pt [6]. These features can make the potential use of Pd feasible and attractive for large-scale fuel cell applications.

It is acknowledged that the ORR activity depends significantly on the crystallographic orientations of a catalytic material. It is reported that the ORR activity of Pd(1 0 0) is much larger than the Pd(1 1 0) and Pd(1 1 1) ones. More specifically, the Pd(1 0 0) activity is fourteen and three times larger than the Pd(1 1 1) and the Pt(1 1 1) ones respectively [7]. Nowadays, by the adoption of novel techniques for the synthesis of nano-catalysts of tailored shapes and sizes, it is possible to induce specific crystallographic faces to be exposed at the reactants. Recently, an enhanced ORR activity of Pd nanocubes, presenting preferentially the (1 0 0) order on the surface in acidic and alkaline medium has been reported [8–10]. Another factor limiting the use of Pd electro-catalysts in fuel cells is their scarce electrochemical stability at high potentials, such as those occurring in polymer electrolyte fuel cells under open circuit voltage (OCV) and starvation condition [11]. Whereas, much lower electrochemical potentials are experienced by cathodes used in DMFCs where methanol cross-over mitigates the oxidative environment.

The common strategy adopted for increasing the activity and stability for the ORR is to disperse the catalytic nanoparticles on supports having high electrical conductivity, large specific surface area [12], and sufficient mechanical stability [13]. In this regard, the high surface area (theoretical value of $2630 \, m^2 \, g^{-1}$), the high conductivity, and the potentially low-cost manufacturing make reduced graphene oxide (rGO) an optimal candidate for the purpose. Systems coupling graphene with Pt have already exhibited an enhanced electro-catalytic activity for the oxidation of small organic molecules [14]. However, this evidence is still controversial; in fact, reports that graphene-supported catalysts have similar or lower activity than carbon supported catalysts for the ORR [15]. For this reason, in the present study, rGO was produced to be coupled with Pt and Pd nano-catalysts to enhance the knowledge on the subject and develop low-cost rGO based fuel cell electrodes of improved efficiency [16]. More specifically, for this study, Pd nanobars were synthesized by the polyol method and deposited both on C and rGO previously synthesized via wet chemistry. For comparison purposes, the same experiments were carried out with Pt nanoparticles, again synthesized by polyol process and deposited on identical substrates. These catalytic electrodes were characterized for the ORR with a Rotating Disk Electrode (RDE) technique in acidic media and, arranged in a DMFC configuration employing a commercial PtRu alloy as anodic electro-catalyst, tested as cathodic catalysts in a real fuel cell environment. The catalysts were physico-chemically characterized by Electron Micro Gravimetric Analysis (TGA), X-Ray Diffraction (XRD) and Transmission Electron Microscopy (TEM).

2. Experimental

2.1. Preparation of chemically reduced graphene oxide

Graphene oxide (GO) was prepared from graphite (Alfa Aesar, 99.9995%) by modified Hummers oxidation method as described previously [17]. Basically, 1 g graphite powder was oxidized with H_2SO_4 98% (25 mL) and $KMnO_4$ (3 g, Aldrich) at 308 K for 3 h. Further, the mixture was diluted with deionized water while maintaining the temperature below 363 K. Successively, 30% H_2O_2 was added to the mixture. The mixture was filtered, purified with HCl and washed with deionized water till neutral pH was reached and dried at 323 K for 24 h. A typical procedure for chemical conversion of GO into rGO requires the dispersion of graphite oxide (0.1 mg mL^{-1}) in water by sonication treatment for 1 h. The

standard way to convert graphene oxide to graphene is based on a chemical reduction in water based on hydrazine hydrate [18]. Green chemical reduction was preferred in this study by using ascorbic acid (w/w of 20:1) as reducing agent for 24 h at room temperature, under mechanical stirring. The rGO was isolated by filtration, washing with water and vacuum drying at 323 K for 24 h.

2.2. Synthesis of catalysts

The Pd-nanobar-based catalyst was synthesized by using a modification of a previously reported method to obtain Pd nanoparticles [19,20]. In the case of the Pd/C and Pd/rGO catalysts, of ethylene glycol (10 mL, EG, J.T. Baker, 99.9%) was placed in a 25-mL three-neck flask equipped with a reflux condenser and a Teflon-coated magnetic stirring bar. The flask was heated in static air under magnetic stirring at 373 K. Na_2PdCl_4 (0.097 g, Sigma–Aldrich, 98%) and KBr (1.2 g, J.T. Baker, 99%) were dissolved in deionized water (6 mL). Meanwhile, polyvinylpyrrolidone (0.183 g, PVP, Aldrich, Mw = 55,000) was dissolved in EG (6 mL) at room temperature. These two solutions were then injected simultaneously into the flask using a two syringe pumps (Cole Palmer Instruments Company, U.S.A.) at a rate of 90 mL h^{-1}. The reaction mixture was heated at 373 K while C (or rGO) (0.05 g) previously heat treated at 550 K for 3 h was added during the reduction process. After 1 h, the reaction was cooled to room temperature and stirred overnight. Then, the product was collected by filtration and washed with bi-distilled water to remove most of the EG and excess PVP. Finally, the product was dried at 340 K for 15 h. A similar process was employed to produce the Pt/C and Pt/rGO catalyst, except that the KBr (J.T. Baker, 99%) was not added in the Pt precursor solution, which consisted on H_2PtCl_6 38.5 mM (6 mL).

2.3. Physico-chemical characterization

The reduced graphene oxide material was investigated by thermogravimetry (TGA) (Q50, TA Instruments, under nitrogen flow at a scanning rate of 10 °C min^{-1}), X-Ray Diffraction (XRD) (D2 Phaser, Bruker, using Cu Kα radiation at 30 kV), and Raman spectroscopy (inVia Renishaw, 514.5 nm incident laser light).

The crystallinity of the catalysts was investigated using a Philips X'Pert X-ray diffractometer, operated using Cu Kα radiation at 30 kV and 30 mA over a 2θ range of 20–90°, step time of 0.5° 2θ min^{-1}, angular resolution of 0.005° 2θ. The diffraction patterns were fitted to Joint Committee on Powder Diffraction Standards (JCPDS) and crystalline size was calculated using line broadening analysis (LBA). For Transmission Electron Microscopy (TEM) analyses (Philips CM12), the specimens were prepared by ultrasonic dispersion in isopropyl alcohol and depositing a drop of suspension on a carbon-coated grid. Thermo Gravimetric (TG) Analysis of the prepared catalysts (TA Instruments, Q500) was performed at a heating rate of 10 K min^{-1} under an air flow rate of 60 cm^3 min^{-1}.

2.4. Electrochemical characterization

All RDE measurements were conducted by a potentiostat/galvanostat Autolab PGSTAT302, in a three-electrode cell at room temperature. A Hg/Hg$_2$SO$_4$ electrode saturated with K$_2$SO$_4$, and a platinum foil electrode were used as the reference electrode and counter electrode, respectively. The working electrode was prepared using a glassy carbon disc (GCD, Radiometer Analytical, S.A.S., model BM-EDI101) measuring 3 mm in diameter, which was previously polished with alumina powder (0.05 μm), sonicated for 10 min, and washed with deionized water. The catalyst thin film was formed on the surface of GCD electrode by transferring catalytic ink (3 μL) and air-drying. The ink was obtained by dispersing the electro-catalyst (3.0 mg) in isopropyl alcohol (220 μL, Baker, 99.9%)

and further addition of Nafion® solution (42 μL, 5 wt.% Ion Power). The RDE experiments were performed in 0.5 M H_2SO_4 previously saturated with O_2 for 20 min at a scan rate of 20 mV/s.

2.5. DMFC testing system

The fuel cell test station system used in this study was from Fuel Cell Technologies, Inc. The test station controlled the flow rate, temperature, pressure and humidity of the oxygen flowing in the cathode, as well as the cell operating temperature. In this case, dry oxygen was used as oxidant at the cathode. Methanol was pumped to the anode side of the fuel cell using a peristaltic pump (FMI Lab Pump, model QVG50). A LabVIEW 5.1.1 software was used in the data acquisition system to control and measure the parameters of the fuel cell. For the polarization measurements, the fuel cell testing system was coupled with a potentiostat.

2.6. Fuel cell setup and membrane electrode assembly (MEA) preparation

The 5 cm^2 fuel cell was used in all the experiments. It consisted of two stainless steel end plates and two graphite plates machined with serpentine flow fields. Two Teflon® gaskets were employed to ensure uniform MEA/GDL compression and to prevent damage to the MEA. The same Pt:Ru (1:1 at.) anode was used in all experiments. Nafion® 117 was used as the electrolyte. Only the type of cathode catalyst was varied. HT-ELAT (E-TEK) was used as the gas diffusion layer (GDL) at the anode side, whereas LT-ELAT (E-TEK) was employed for the cathode. The GDL was painted with the catalytic ink composed of catalyst (67%) and Nafion® (33%). The membrane and electrodes were joined by hot-pressing method. Before polarization measurements, membrane rehydration and catalysts activation was performed. The membrane rehydration was carried out by feeding the anode with 5 mL/min of bi-distillate water for 15 min at room temperature. The catalyst activation was carried out by running a chrono-amperometry at 0.2 V for 2 h while 3 mL/min of 1 M methanol was fed to the anode.

3. Results and discussion

3.1. Characterization of rGO material

The thermal behavior of graphene oxide and reduced graphene oxide was studied by TG analysis (see supplementary file, Fig. S1). It was observed that GO material had much lower thermal stability than graphite due to the introduction of oxygen-containing groups. The labile groups were observed to be removed around 573 K and the stable ones were decomposed around 973 K. Upon green chemical reduction, rGO resulted more stable than GO but still did not reach the thermal stability of graphite due to the residual functional groups.

The XRD analysis (see supplementary file, Fig. S2) showed that with respect to graphite, the typical (0 0 2) diffraction peak was down-shifted to 2θ values of 10.5° for GO material and up-shifted to 20.8° for rGO. These shifts together with the decrease of corresponding interlayer spacing value from 0.83 nm for GO to 0.44 nm for rGO confirm the partial removal of functional groups.

Further, the nature of disorder in GO and rGO materials was studied by Raman spectroscopy (see supplementary file, Fig. S3). The typical D and G bands are identified although they present some shift with respect to those of graphite. The blue shift to higher frequencies for G band is accounted by the appearance of amorphous domains in GO material, which also causes the increase of I_D/I_G ratio (I is Raman intensity). A further increase in I_D/I_G ratio was observed upon reduction of GO confirming desorption of oxygen
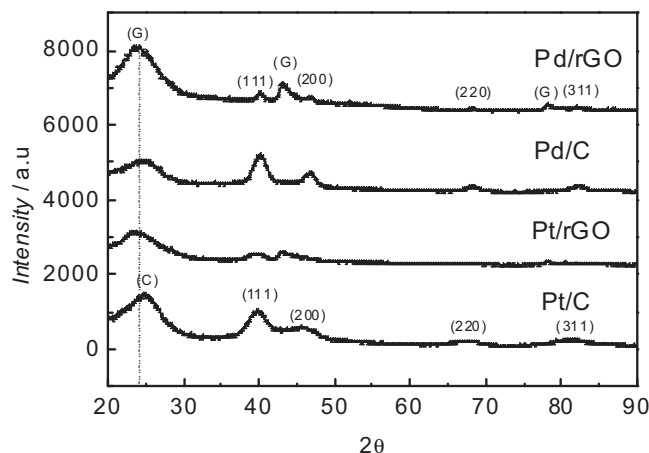

Fig. 1. XRD patterns for Pd/C, Pt/C, Pd/rGO, and Pt/rGO catalysts.

bonded saturated sp^3 carbons and appearance of defects. Anyhow, this increase is indicative of decrease in the size of sp^2 domains but increase in their number. Although still poor, the restoration of electronic conjugation is to be improved by further thermal treatment during catalysts synthesis.

3.2. Physico-chemical characterization of catalysts

3.2.1. XRD analysis

The XRD patterns of the Pd/C, Pd/rGO, Pt/C, Pt/rGO are shown in Fig. 1. In general, the patterns of the Pd catalysts have crystalline structure with peaks appearing at 40.119°, 46.659°, 68.121°, 82.1° and 86.619°, corresponding to the (1 1 1), (2 0 0), (2 2 0) and (3 1 1) planes of face-centered cubic structure (fcc) of Pd (JCPDS 46-1043) while the diffraction peaks observed at 39.5°, 46.8° and 67.6° correspond to the (1 1 1), (2 0 0) and (2 2 0) planes of the fcc structure of Pt (JCPDS 87-0646). The diffraction peaks at about $2\theta = 25°$, 43° and 78° in the Pd/rGO and Pt/rGO catalysts were assigned to the reflections of the graphene support. The average crystal size was calculated based on the broadening of the (1 1 1) diffraction peak according to the Scherrer equation such as 4.9, 9.9, 2.7 and 3.3 nm for Pd/C, Pd/rGO, Pt/C and Pt/rGO catalysts, respectively. Furthermore, the Pd(1 1 1)/Pd(1 0 0) ratio was estimated 2.21 and 2.36 for Pd/C and Pd/rGO, respectively. These ratios are lower than the theoretical value 2.38 reported for the polycrystalline Pd with typical fcc structure [21]. This result evidenced the preferential exposition of Pd(1 0 0) surface for the Pd catalysts.

3.2.2. Thermo Gravimetric Analysis

TGA analyses were carried out in order to estimate the effective metal load on the support (Fig. 2). For the carbon-supported catalysts, the curves can be divided in three distinct regions: the first slight loss at temperatures below 600 K possibly was caused by the evaporation of adsorbed water and carbonaceous residues from the catalyst preparation. The second region consists of a significant decrease in the weight fraction in the range of 650–870 K, which is mainly associated with the decomposition of the carbon material by reacting with O_2 to form CO_2 at temperatures above 870 K. The third section corresponds to the near stable weight fractions at temperatures higher than 870 K. A slight weight gain through the third region was observed for all synthesized catalysts and could be related to the phenomenon of Pd or Pt oxidation. This weight gain was more evident in the Pt/C catalyst. However, the first point in the third temperature section was taken as the actual Pd or Pt load value for the corresponding catalyst, where Pd and Pt oxidation occurs to a lesser extent, thus minimizing the error due
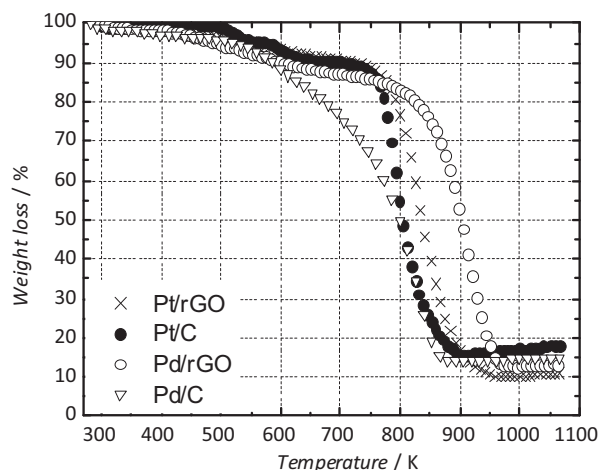
Fig. 2. Weight loss obtained by TGA analysis for the synthesized catalysts.

to the oxidation process. In the case of the rGO-supported catalysts, the second region started and finished at higher temperature (850–950 K) compared to the carbon-supported catalysts region (650–870 K). This result was expected and showed the higher thermal stability of the graphene nano sheets compared to Vulcan carbon black. The real metal loading was 12, 16.7, 14.5 and 13.3% for the Pt/rGO, Pt/C, Pd/C and Pd/rGO, respectively. Significant

differences were observed in the thermal profiles of Pd-based catalysts; whereas, very small differences were recorded for the Pt catalysts. Since the decomposition of a carbonaceous substrate is strongly catalyzed by the presence of a noble metal, especially from the metal-carbon interaction [22]. The higher decomposition temperature for the Pd/rGO catalysts could evidence a low affinity between the Pd structure and the non-functionalized graphene surface. We think that this poor affinity between Pd nanobars and graphene is essentially related to the lower adsorption characteristics of Pd precursor and the lack of functional groups on the graphene surface. However, a low metal–support interaction can increase the number of catalytic sites available for the process, considering the high tendency of functional groups and foreign species to be adsorbed on the Pd(1 0 0) surface [19]. This aspect appears relevant to the ORR.

3.2.3. TEM results

TEM experiments were carried out in order to observe the shape, size and dispersion of the synthesized Pd and Pt nanoparticles over the support (Fig. 3). The average Pt particle size for the Pt/C and Pt/rGO catalysts were 2.9 and 3.1 nm, respectively. These values are in good agreement with the previous ones calculated from XRD by using the Scherrer equation. In addition, excellent Pt dispersion was achieved over the Vulcan carbon black and graphene, as can be observed in Fig. 3a and c, respectively. The TEM images indicate that the Pt catalysts are composed of irregularly, meanly
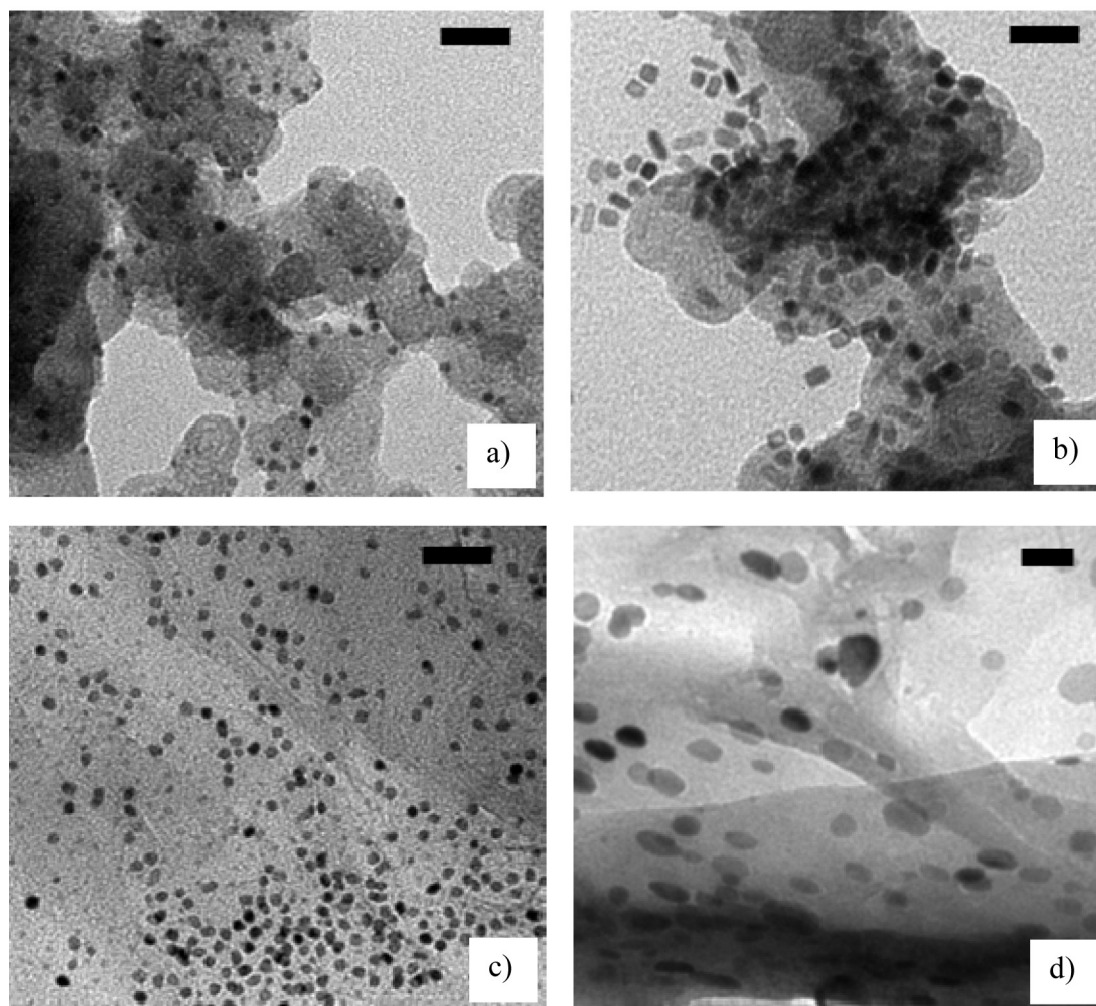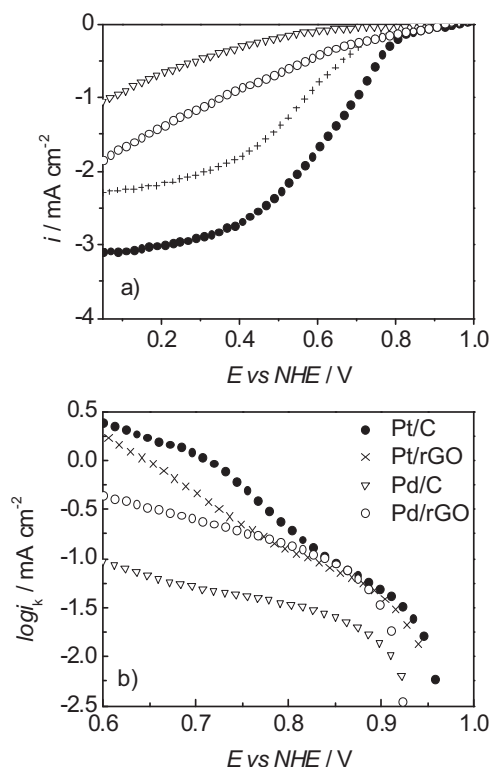

Fig. 3. TEM images of (a) Pt/C, (b) Pd/C, (c) Pt/rGO and (d) Pd/rGO. Scale bar: 20 nm.

Fig. 4. (a) Comparison of the RDE curves of the synthesized catalysts at 1200 rpm at room temperature and (b) corrected current ($\log i_k$) Tafel plots for the synthesized catalysts at room temperature.

Table 1
Maximum power density and cell voltage found with 1 M methanol concentration at different temperatures.

	MPD/E_{cell} [Wg$_{Pd or Pt}^{-1}$ V^{-1}] 1 M		
	303 K	343 K	363 K
Pt/C	6.26/0.18	11.24/0.18	10.64/0.18
Pt/rGO	2.6/0.17	10.21/0.18	9.69/0.19
Pd/C	0.71/0.24	1.9/0.23	1.2/0.15
Pd/rGO	1.6/0.23	2.75/0.17	2.61/0.21

activity order is as follows: Pt/C > Pt/rGO > Pd/rGO > Pd/C. A Tafel slope of 61 and 60 mV dec^{-1} was calculated for Pt/C and Pt/rGO catalysts at high potentials (∼0.9–0.8 V), and 128 and 135 mV dec^{-1} at medium potentials (0.8–0.7 V). In the case of Pd catalysts, the Tafel slope was 65 and 71 mV dec^{-1} at high potentials. Tafel slopes of 60 and 120 mV (for high and medium potential region, respectively) are characteristic for O_2 reduction on Pd and Pt catalysts [9]. The change in the slope has been attributed to the modification from Temkin to Langmuir conditions for the adsorption of reaction intermediates. However, the transfer of the first electron to O_2 is often assumed as the rate determining step in both regions [10]. The Tafel slope values obtained in this work suggest that the reaction mechanism is the same on Pt/C and Pt/rGO catalysts. Pd catalysts are characterized by lower intrinsic activity for ORR compared to Pt. The performance of the graphene-supported Pd catalyst is better than that of Pd supported on carbon black despite its larger particle size. This is a clear indication of a better specific activity due to a larger occurrence of Pd(1 0 0) planes on the surface and lower interaction with the support that provides a larger availability of catalytic sites for the ORR. Such an evidence indicates that the activity of Pd/graphene may be further increased, provided that smaller mean particle size is obtained, compared with the optimum size of Pd nanobar for this reaction (48 nm) [8]. Quite different evidence is observed for Pt where the anchoring effect of functional groups on carbon black and the different crystallographic orientation, required to enhance the ORR, play a relevant role [7]. Graphene support has also received particular attention recently for fuel cell applications due to its exceptional physico-chemical properties, such as extremely theoretically high surface area, superior electronic conductivity, large surface to volume ratio and high stability [23]. Considering these interesting properties, superior electro-activity would be expected from these graphene-based catalysts compared to carbon-based. Such improved behavior has been observed for some reactions, such as methanol, ethanol, and ethylene-glycol electro-oxidation reaction [24,25]. However, controversial results regarding the activity for ORR have been obtained from half-cell experiments: higher [26,27], similar [28], and lower [15] ORR electro-activity than C-based catalysts has been observed. Furthermore, fuel cell tests with Pt catalysts supported on rGO, used as cathode material, have shown lower performance than the Pt catalysts supported on C. It was believed that the ORR diffusion-limiting currents were strongly affected by the structure of the catalyst supporting material [29]. The sheet structure of graphene, with small particles entrapped within the fold of these foils, might block oxygen compared with spherical carbon black particles, with nanosized metal catalyst allocated on the edges of these spheres [15]. Thus, flat structure of graphene may be less effective for nanosized Pt particles than the spherical structure of carbon blacks, randomly distributed in the catalyst layer. Even though excellent dispersion and similar particle size were observed by TEM and XRD analyses for the Pt catalysts, the electrocatalytic activity of the rGO-supported was lower than the C-supported catalyst. The above hypothesis can explain the lower performance for the Pt/rGO obtained in the present work. In the case of Pd, some degree of

spherical, shaped Pt nanoparticles, while the Pd catalysts had square shape nanoparticles similar to nanobars or nanorods. As shown in Fig. 3b, most of the nanoparticles over the carbon support consisted of Pd nanobars with particle size from approximately 4 × 4 nm to 4 × 10 nm (width × length). This implies that compared to the previous synthesis of unsupported nanobars, where the particle size was ∼8 × 8 nm to 8 × 10 nm, similarly shaped and thinner Pd-nanobars were successfully prepared and supported on carbon black [19]. On the other hand, the Pd nanoparticles in the Pd/rGO catalyst have a mixture of irregular and square shapes. The size for the nanoparticles was approximately from 4 × 4 nm to 8 × 15 nm. Even though the same synthesis method to produce Pd/C and Pd/rGO was employed, the differences in size and shape suggest that rGO plays a different role during the nanobars formation, perhaps modifying the nucleation and reduction kinetics which are critical for the unidirectional growth. This is essentially determined by the presence or absence of carbon functional groups on the surface which may act as anchoring centers as well as nucleation sites. Furthermore, the more defined square shape found in the Pd/C catalyst corroborated the lower Pd(1 1 1)/Pd(1 0 0) ratio calculated by XRD, compared to Pd/rGO catalyst.
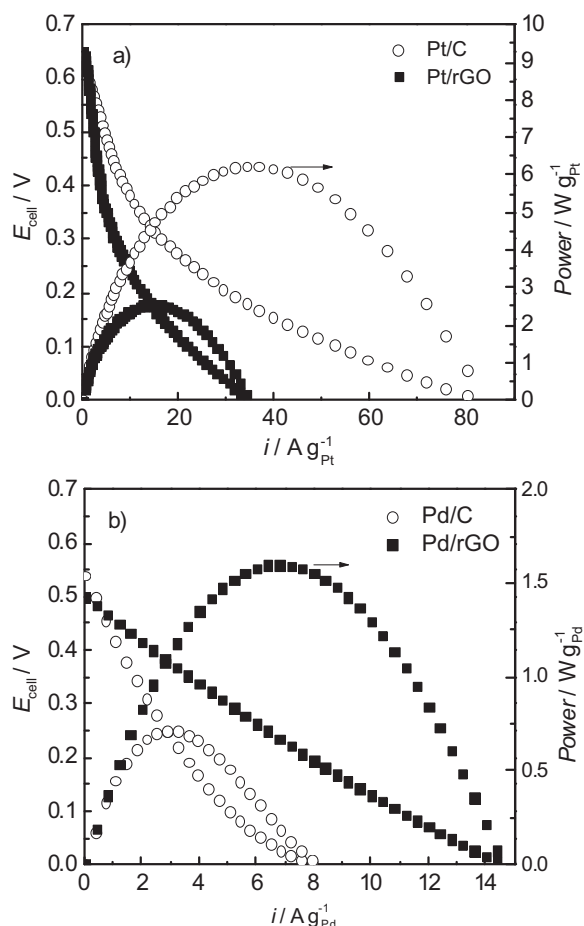
3.3. RDE measurements

Fig. 4 shows a comparison for the ORR of all the synthesized catalysts under similar experimental conditions. From Fig. 4, the ORR on the Pt catalysts is diffusion-controlled when the potential is less than 0.4 V, and is under mixed diffusion kinetic control in the potential region between 0.4 and 0.8 V. When the potential is higher than 0.8 V, the ORR is under kinetic control, in the Tafel region. On the other hand, the polarization curves of the Pd catalysts show a mixed control over the potential range, not reaching a well-defined current density in the diffusion-limited region. Therefore, the ORR

Fig. 5. Polarizations curves obtained for (a) the Pt-Based catalysts and (b) Pd-based catalysts. Conditions: temperature: 303 K, anode: 3 mL methanol solution/min (1 M). Cathode: 100 mL O_2/min at atmospheric pressure. Membrane: Nafion 117®.

agglomeration is observed in the case of carbon black support; whereas, this does not seem to be the case for rGO-based catalyst. It is pointed out that, as above discussed; an increment of electrocatalytic activity can be appreciated in the Pd/rGO catalyst compared to Pd/C catalyst (Fig. 4). This is explained by the shape and size of the Pd particles. Recently, it has been reported that the kinetic performance of Pd for the ORR in acidic medium is size dependent [8]. Beside the above considerations, the higher activity of the Pd/rGO than Pd/C catalysts can be associated to the differences in the catalyst morphology discussed in Section 3.2.3.

3.4. Fuel cell performance

Fig. 5 shows the typical polarization and power density curves obtained for the synthesized Pt and Pd catalysts. The experiments were carried out with 1 M methanol concentration at different temperatures. These data are summarized in Table 1. The maximum power density (MPD) was about 2.4 times higher for the Pt/C catalysts, compared to the Pt/rGO at 303 K, with 1 M methanol solution fed to the anode. Moreover, it can be noted that higher performance was obtained for the Pt/C than Pt/rGO in all the conditions studied. On the contrary, the corresponding performance for the Pd supported over rGO was 2.2 times higher than the Pd supported on carbon-Vulcan at the same conditions. The values recorded at 363 K are lower than those at 343 K due to the dehydration of the membrane at that temperature produced by the use of dry oxygen at

the cathode. This dehydration produces an increase of the series resistance in the Nyquist plot (not shown).

4. Conclusions

Reduced graphene oxide (rGO) was synthesized in this study to improve the catalytic properties of Pd as an alternative to conventional carbon black (C) substrates. Pd nanobars and Pt nanoparticles were synthesized by the polyol method and deposited for comparison both on commercial C and rGO. The electro-catalytic activity of the electrode is importantly affected by the support chosen. Specifically, the Pd nano-catalyst proved an enhanced performance when on rGO, while the Pt counterpart was found being more active when placed on C. The results suggest that the ORR activity depends strongly on the intrinsic catalytic activity of the metal, crystallographic orientation of the active phase, metal support interaction and morphology of the catalytic phase and support.

Appendix A. Supplementary data

Supplementary data associated with this article can be found, in the online version, at http://dx.doi.org/10.1016/j.apcatb.2013.07.057.

References

[1] L. Calvillo, V. Celorrio, R. Moliner, A.B. Garcia, I. Cameán, M.J. Lazaro, Electrochimica Acta 102 (2013) 19–27.
[2] H.A. Gasteiger, S.S. Kocha, B. Sompalli, F.T. Wagner, Applied Catalysis B: Environmental 56 (2005) 9–35.
[3] E. Antolini, Energy and Environmental Science 2 (2009) 915–931.
[4] X. Fu, Y. Liu, X. Cao, J. Jin, Q. Liu, J. Zhang, Applied Catalysis B: Environmental 130/131 (2013) 143–151.
[5] J.S. Doa, Y.T. Chena, M.H. Lee, Journal of Power Sources 172 (2007) 623–632.
[6] Z. Zhang, L. Xin, K. Sun, W. Li, International Journal of Hydrogen Energy 36 (2011) 12686–12697.
[7] M. Shao, Journal of Power Sources 196 (2011) 2433–2444.
[8] C.L. Lee, H.P. Chiou, Applied Catalysis B: Environmental 117/118 (2012) 204–211.
[9] H. Erikson, A. Sarapuu, N. Alexeyeva, K. Tammeveski, J. Solla-Gullón, J.M. Feliu, Electrochimica Acta 59 (2012) 329–335.
[10] H. Erikson, A. Sarapuu, K. Tammeveski, J. Solla-Gullón, J.M. Feliu, Electrochemistry Communications 13 (2011) 734–737.
[11] N.A. Karim, S.K. Kamarudin, Applied Energy 103 (2013) 212–220.
[12] D. Sebastián, A. García-Ruíz, I. Suelves, R. Moliner, M.J. Lázaro, V. Baglio, A. Stassi, A.S. Aricò, Applied Catalysis B: Environmental 115/116 (2012) 269–275.
[13] G. Carotenuto, S. De Nicola, M. Palomba, D. Pullini, A. Horsewell, T.W. Hansen, L. Nicolais, Nanotechnology 23 (2012) 485705 (8 pp.).
[14] S. Bong, Y.R. Kim, I. Kim, S. Woo, S. Uhm, J. Lee, H. Kim, Electrochemistry Communications 12 (2010) 129–131.
[15] E. Antolini, Applied Catalysis B: Environmental 123/124 (2012) 52–68.
[16] A. Pruna, D. Pullini, D. Busquets, The Journal of Nanoparticle Research 15 (2013) 1605 (11 pp.).
[17] F.R.F. Fan, S. Park, Y. Zhu, R.S. Ruoff, A.J. Bard, Journal of the American Chemical Society 131 (2009) 937–939.
[18] D.A. Stankovich, R.D. Dikin, K.A. Piner, A. Kohlhaas, A. Kleinhammes, Y. Jia, Y. Wu, S.T. Nguyen, R.S. Ruoff, Carbon 45 (2007) 1558–1565.
[19] Y.J. Xiong, H.G. Cai, B.J. Wiley, J.G. Wang, M.J. Kim, Y.N. Xia, Journal of the American Chemical Society 129 (2007) 3665–3675.
[20] R. Carrera-Cerritos, M. Guerra-Balcázar, R. Fuentes Ramírez, J. Ledesma-García, L.G. Arriaga, Materials 5 (2012) 1686–1697.
[21] Y. Xiong, J.M. McLellan, Y. Yin, Y. Xia, Angewandte Chemie: International Edition 46 (2007) 790–794.

[22] A.S. Aricò, P.L. Antonucci, V. Antonucci, in: A. Wieckowski, E.R. Savinova, C.G. Vayenas (Eds.), Catalysis and Electrocatalysis at Nanoparticle Surfaces, Marcel Dekker Inc, New York, 2003.

[23] H. Huang, H. Chen, D. Sun, X. Wang, Journal of Power Sources 204 (2012) 46–52.

[24] Z. Wen, S. Yang, Y. Liang, W. He, H. Tong, L. Hao, X. Zhang, Q. Song, Electrochimica Acta 56 (2010) 139–144.

[25] R. Awasthi, R.N. Singh, International Journal of Hydrogen Energy 37 (2012) 2103–2110.

[26] M.H. Seo, S.M. Choi, J.K. Seo, S.H. Noh, W.B. Kim, B. Han, Applied Catalysis B: Environmental 129 (2013) 163–171.

[27] Y. Xin, J. Liu, Y. Zhou, W. Liu, J. Gao, Y. Xie, Y. Yin, Z. Zou, Journal of Power Sources 196 (2011) 1012–1018.

[28] H. Wu, D. Wexler, H. Liu, Journal of Solid State Electrochemistry 15 (2011) 1057–1062.

[29] A.H.A. Monteverde Videla, L. Zhang, J. Kim, J. Zeng, C. Francia, J. Zhang, S. Specchia, Journal of Applied Electrochemistry 43 (2013) 159–169.